Hydrogen storage in Ti-Hf-Fe-Ni alloys

José Núñez
IFUAP-BUAP, Mexico

Tuur Boonen
Faculty of Science, University of Antwerp, Antwerp, Belgium

Seppe Lefevere
Faculty of Science, Ghent University, Gent, Belgium

(Computational Materials Physics by Stefaan Cottenier)
(Dated: December 6, 2025)

This study uses density functional theory to investigate Ti–Hf–Fe–Ni alloys for hydrogen storage. Formation energies confirm the thermodynamic stability of several phases, while hydrogen insertion into interstitial sites reveals preferred positions, lattice expansion, and storage capacity. Certain interstitial sites provide enhanced hydrogen stability, and vacancies further increase hydrogen insertion, offering guidance for designing efficient hydrogen-storage alloys.

I. INTRODUCTION

Hydrogen-storage materials continue to attract attention as clean-energy technologies advance [1, 2]. Intermetallic alloys play an important role in this search [3]. Alloys based on Ti, Fe, Hf and Ni are especially interesting because they pair lightweight elements with transition metals that form stable intermetallic compounds [4]. These crystal structures provide several interstitial sites that can hold hydrogen [2]. However, hydrogen storage capacity depends strongly on phase stability and local atomic environments. [5]. This work uses density functional theory (DFT) to examine the structural and energetic behaviour of these alloys. By comparing variations in crystal structure, composition, and vacancy behavior, together with their interactions with hydrogen, we can determine which material phases are most favorable for efficient hydrogen storage.

II. METHODOLOGY

All calculations were performed within DFT [6, 7], using the Perdew–Burke–Ernzerhof (PBE) exchange–correlation functional under the generalized gradient approximation (GGA) [8], as implemented in the Quantum ESPRESSO package [9]. Scalar-relativistic pseudopotentials were used for all atoms [10–12]. Convergence tests were performed assuming ferromagnetic order. The convergence threshold for self-consistency was established at 1×10^{-12} Ry. The cutoff energy was set to 140 Ry and 840 Ry for the wavefunctions and charge density, respectively. A k-mesh of $14 \times 14 \times 14$ was selected, as smaller values yield residual magnetic moments. For the smearing, a 0.01 Ry gaussian spreading was used. For the hydrides, a full geometry relaxation was performed with a convergence threshold on the pressure for variable cell relaxation of 0.1 kbar.

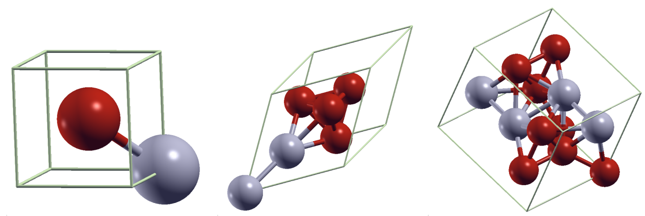

(a) Pm$\bar{3}$m (AB), cubic, No. 221. (b) Fd$\bar{3}$m (AB_2), cubic, No. 227. (c) P6_3/mmc (AB_2), hexagonal, No. 194.

FIG. 1: The three crystal structures treated in this work. The gray and red spheres represent the A and B atoms, respectively, listed in table I.

III. RESULT AND DISCUSSION

According to the third-order Birch–Murnaghan equation of state (B-M EOS) [13, 14], the found equilibrium volume of TiFe, $V_{\mathrm{eq}} = 174.7362$ a.u.^{3}, agrees with previous theoretical results [15, 16]. The corresponding bulk modulus, $B_0 = 190.911$ GPa, is also consistent with the reported values [15]. Figure 2 presents the calculated data points for the $E(V)$ curve alongside the B-M EOS fit. A subsequent full geometry relaxation returns an equilibrium volume of $V_{\mathrm{eq}} = 174.6769$ a.u.^{3}, in agreement with the first value. When pressure is applied to the crystal, its volume decreases. In the case of TiFe, an applied pressure of 100 kbar is predicted to cause a volume reduction of approximately 5%.

To provide a consistent reference for this work, the study focuses on the pristine binaries TiFe, TiNi, HfFe, and HfNi. Three crystal structures will be considered in this work, depicted in Figure 1. Previously, TiFe convergence testing was performed in the cubic crystal system Pm$\bar{3}$m (also known as the B2 structure), depicted in figure 1a. The second and third systems are cubic Fd$\bar{3}$m (figure 1b), and hexagonal P6_3/mmc (figure 1c).

A, B	structure	a [a.u.]	c/a	B_0 [GPa]	E_f [kJ/mol]	m [μ_B/cell]	mag. order
Ti, Fe	Pm$\bar{3}$m (AB)	5.5906	1.00	190.911	-39.7453	0.00	non-magnetic
	Fd$\bar{3}$m (AB_2)	12.7786	1.00	154.197	-28.6763	0.00	non-magnetic
	$P6_3$/mmc (AB_2)	9.0285	1.62	-	-27.9010	10.58	ferromagnetic
Ti, Ni	Pm$\bar{3}$m (AB)	5.6980	1.00	158.443	-34.2273	5.54	ferromagnetic
	Fd$\bar{3}$m (AB_2)	12.6988	1.00	181.136	-34.7828	0.00	non-magnetic
Hf, Fe	Pm$\bar{3}$m (AB)	5.9118	1.00	172.516	-36.8701	0.00	non-magnetic
	Fd$\bar{3}$m (AB_2)	13.1860	1.00	163.357	-36.2814	6.35	ferromagnetic
	$P6_3$/mmc (AB_2)	9.3352	1.62	-	-33.6961	12.16	ferromagnetic
Hf, Ni	Pm$\bar{3}$m (AB)	5.9959	1.00	151.987	-45.6349	0.00	non-magnetic
	Fd$\bar{3}$m (AB_2)	13.0717	1.00	177.392	-49.4347	0.00	non-magnetic

TABLE I: Structural parameters, bulk moduli, formation energies, and magnetic properties of Ti–Fe–Hf–Ni compounds in different crystal structures.

The formation energies were calculated with respect to their respective A and B elements [17], as:

$$E_f(\mathrm{AB}) = E(\mathrm{AB}) - [E(\mathrm{A}) + E(\mathrm{B})]$$

A negative formation energy indicates that the compound is thermodynamically stable and will not decompose into its elemental constituents. The calculated results for all pristine structures studied are summarized in table I. For reference, the experimental value for TiFe (Pm$\bar{3}$m) is -31 kJ/mol [18] while our calculations are -39.7 kJ/mol. Furthermore, all calculated formation energies are negative, demonstrating that the compounds are thermodynamically stable relative to their elemental constituents. These results are also in good agreement with the Materials Project data [19], which reinforces the reliability of our DFT calculations. It should be noted that, according to the literature, some compounds are ferrimagnets, for example HfFe2 (hexagonal). We did not calculate structures with this magnetic ordering.

To investigate the hydrogen storage behavior of the Ti–Fe–Hf–Ni alloys, hydrogen atoms were systematically inserted into the available interstitial sites of each crystal structure. For the Pm$\bar{3}$m phases, the high-symmetry Wyckoff positions 3c, 3d, 6f, and 8g were examined, while for the Fd$\bar{3}$m structures the relevant 8a, 16d were considered. The thermodynamic stability of each hydride is quantified via the formation energy. The formation energies were calculated with respect to their respective A and B elementals and the number of H2 molecules (x) [17], as:

$$E_f(\mathrm{ABH}_x) = E(\mathrm{ABH}_x) - \left[E(\mathrm{A}) + E(\mathrm{B}) + \frac{x}{2}E(\mathrm{H}_2)\right]$$

The results in Tables II and III show that only a subset of Wyckoff sites produce stable hydride configurations. Hydrogen insertion generally induces a local lattice expansion, the magnitude of which depends both on the occupied site and on the chemical environment. In some cases, inserting hydrogen changes the magnetic moments and highlights the connection between magnetic and structural properties.

Several Ti–Fe–Hf–Ni compounds were compared, with the focus on the different interstitial sites that can accommodate hydrogen atoms. The goal is to find which combination of crystal structure and Wyckoff position gives the lowest hydrogen insertion energy, and thus the most stable configurations for hydrogen storage. In the Pm$\bar{3}$m (B2-type) phases, hydrogen insertion was tested in the high-symmetry Wyckoff positions 3c, 3d, 6f, and 8g. Among these, the 3c site emerges as the only position that consistently has negative formation energies across all four compositions (TiFe, TiNi, HfFe, and HfNi). This site corresponds to an octahedral interstitial cavity surrounded by a mixed coordination of A and B atoms, providing sufficient free volume and an optimal electronic environment for hydrogen accommodation. TiFeH (3c) stands out among Pm$\bar{3}$m hydrides due to its low formation energy ($E_f = -34.3$ kJ/mol). Combined with abundant, inexpensive elements and strong thermodynamic stability, it emerges as a good candidate for hydrogen storage.

Additionally, hydrogen insertion into the 3c site leads to a moderate lattice expansion (around 9–10%) without inducing magnetic ordering, suggesting a mechanically and magnetically stable hydride phase. In contrast, inserting hydrogen into the 3d, 6f, and 8g sites causes noticeable lattice distortions and, in some cases, small residual magnetic moments. This suggests that hydrogen in these less symmetric positions disrupts the local electronic structure and weakens the metallic bonding. Thus, only certain sites allow energetically favorable hydrogen binding.

The picture becomes more complex in the Fd$\bar{3}$m (cubic Laves phase) structures. Here, both the 8a and 16d sites were investigated, showing a wider range of possible local environments for hydrogen. Hydrogen in the 8a and the 16d–s sites gives negative formation energies, showing that these sites can form stable hydrides, though not as effectively as the 3c site in the B2 phases. Overall, while Fd$\bar{3}$m structures can host hydrogen, the B2-type Pm$\bar{3}$m phases remain the most promising for efficient hydrogen storage.

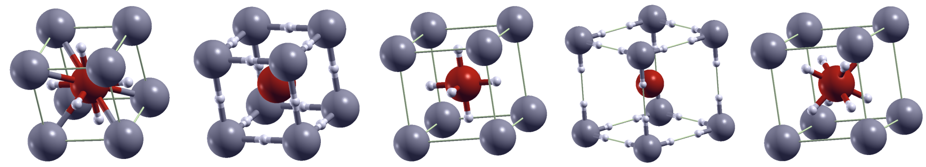

$Pm\bar{3}m$ (AB)	H Wyckoff atoms/cell	3c 5	3d 5	6f 8	6e 8	8g 10
$TiFeH_x$	a [a.u.]	6.1387	6.5118	7.4451	–	7.6092
	m [μ_B/cell]	0.00	2.41	0.01		0.00
	E_f [kJ/mol]	-34.3269	48.6968	289.5192		169.7795
$TiNiH_x$	a [a.u.]	6.1712	6.4765	7.7220	–	7.7061
	m [μ_B/cell]	0.00	0.00	2.09		0.00
	E_f [kJ/mol]	-47.9513	46.0982	239.4867		208.1207
$HfFeH_x$	a [a.u.]	6.3226	6.9295	7.4017	–	7.8358
	m [μ_B/cell]	0.00	2.80	0.00		0.00
	E_f [kJ/mol]	-46.1189	66.3851	270.4636		145.2903
$HfNiH_x$	a [a.u.]	6.3499	6.8869	7.5246	–	7.9553
	m [μ_B/cell]	0.00	0.00	0.00		0.00
	E_f [kJ/mol]	-49.3224	56.2022	255.6766		198.2236

TABLE II: Lattice parameter, magnetic moment and formation energy for different hydrides in the $Pm\bar{3}m$ structure. The H were introduced in Wyckoff positions.

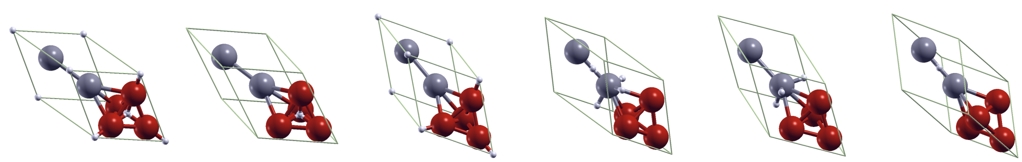

$Fd\bar{3}m$ (AB_2)	H Wyckoff atoms/cell	8a 8	8a-i 7	8a-c 7	16d 10	16d-t 9	16d-s 7
$TiFe_2H_x$	a [a.u.]	13.3528	13.0636	13.0636	13.8306	13.4940	12.9526
	m [μ_B/cell]	4.78	5.29	5.29	8.35	7.40	6.20
	E_f [kJ/mol]	-0.0960	-17.3574	-17.3575	40.5379	18.1308	-15.8301
$TiNi_2H_x$	a [a.u.]	13.3098	–	–	13.6780	13.4329	12.8679
	m [μ_B/cell]	2.12			0.00	0.00	0.00
	E_f [kJ/mol]	-8.3468			25.2543	5.1389	-23.3205
$HfFe_2H_x$	a [a.u.]	13.5907	13.3997	13.3997	14.4969	–	13.3981
	m [μ_B/cell]	5.22	6.16	6.16	8.86		6.81
	E_f [kJ/mol]	-18.8375	-31.1764	-31.1765	59.1169		-17.1218
$HfNi_2H_x$	a [a.u.]	13.5489	–	–	14.3661	–	13.2934
	m [μ_B/cell]	0.00			0.00		0.00
	E_f [kJ/mol]	-25.6436			37.4944		-30.7586

TABLE III: Lattice parameter, magnetic moment and formation energy for different hydrides in the $Fd\bar{3}m$ structure. The H were introduced in Wyckoff positions.

Finally, a vacancy calculation was performed to investigate the effect of point defects on hydrogen insertion in TiFe ($Pm\bar{3}m$ phase). Removing a single Fe atom creates a larger and more favorable interstitial site, significantly enhancing hydrogen binding compared to the perfect lattice. After full relaxation of a $3 \times 3 \times 3$ supercell with the central Fe atom removed, the hydrogen atom remains trapped in the vacancy. The hydrogen insertion energy increases from -34.3 kJ/mol in the perfect lattice to -72.4 kJ/mol in the vacancy. The vacancy provides additional free volume and a lower local electron density, allowing hydrogen to form stronger bonds with the neighboring Ti and Fe atoms. Consequently, the hydrogen atom becomes significantly more stable in the vacancy, suggesting that engineered point defects could be a practical strategy to enhance hydrogen storage capacity and reversibility in TiFe-based hydrides.

IV. CONCLUSION

The DFT calculations demonstrate that Ti–Hf–Fe–Ni alloys form thermodynamically stable phases with significant potential for hydrogen storage. Systematic hydrogen insertion into interstitial sites identifies site- and structure-specific preferences, with the 3c Wyckoff site in the Pm$\bar{3}$m phase providing the most stable and energetically favorable configuration across all compositions. Hydrogen incorporation leads to moderate lattice expansion and can modify magnetic moments. Moreover, introducing vacancies further enhances hydrogen uptake by creating larger, low-electron-density sites, where hydrogen binds more strongly than in the perfect lattice. These results collectively pinpoint the most promising phases, interstitial sites, and defect-engineering strategies for optimizing hydrogen storage, providing a clear roadmap for designing efficient Ti–Hf–Fe–Ni hydrides.

Appendix A: The B-M EOS fit

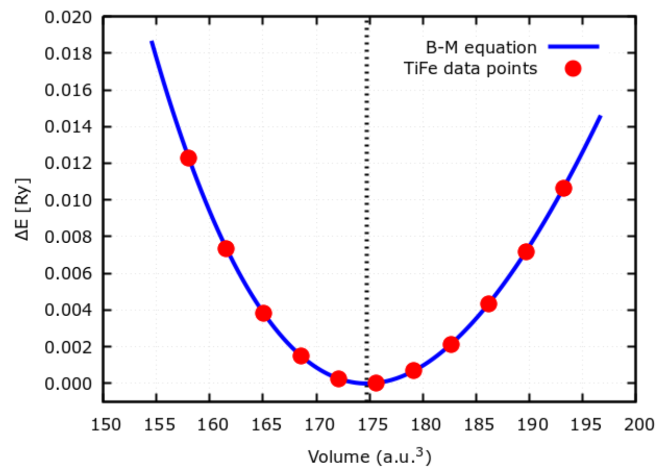

FIG. 2: $E(V)$ graph. The B-M EOS was used to calculate the equilibrium volume and the bulk modulus. Both quantities are in agreement with reported values in the literature. The vertical dashed line indicates the equilibrium volume.

[1] Kumar, A., *et al.*, Coatings **12**, 1813 (2022).
[2] Zhou, L., *et al.*, International Journal of Hydrogen Energy (2025).
[3] Li, H., *et al.*, Journal of Alloys and Compounds **861**, 158497 (2021).
[4] Mizuno, Y., *et al.*, International Journal of Hydrogen Energy **40**, 16707 (2015).
[5] Wang, J., *et al.*, International Journal of Hydrogen Energy **50**, 2517 (2025).
[6] Hohenberg, P., *et al.*, Phys. Rev. **136**, B864 (1964).
[7] Kohn, W., *et al.*, Phys. Rev. **140**, A1133 (1965).
[8] Perdew, J. P., *et al.*, Phys. Rev. Lett. **77**, 3865 (1996).
[9] Giannozzi, P., *et al.*, Journal of Physics: Condensed Matter **29**, 465901 (2017).
[10] Hamann, D. R., Phys. Rev. B **88**, 085117 (2013).
[11] Schlipf, M., *et al.*, Computer Physics Communications **196**, 36 (2015).
[12] Scherpelz, P., *et al.*, Journal of chemical theory and computation **12**, 3523 (2016).
[13] Murnaghan, F. D., Proceedings of the National Academy of Sciences **30**, 244 (1944).
[14] Birch, F., Phys. Rev. **71**, 809 (1947).
[15] Kong, Z., *et al.*, Physica B: Condensed Matter **573**, 13 (2019).
[16] Kang, K., *et al.*, Physica B: Condensed Matter **715**, 417584 (2025).
[17] Chnika, Y., *et al.*, Journal of Molecular Liquids **437**, 128512 (2025).
[18] Gachon, J., *et al.*, Calphad **7**, 1 (1983).
[19] Jain, A., *et al.*, APL Materials **1**, 011002 (2013).